Vibration-dependent photoelectron angular distributions and branching ratios observed across the Cooper-minimum region of bromobenzene

Ivan Powis*
School of Chemistry, University of Nottingham, Nottingham NG7 2RD, United Kingdom

Minna Patanen,† Egill Antonsson,‡ Christophe Nicolas, and Catalin Miron§
Synchrotron SOLEIL, l'Orme des Merisiers, Saint-Aubin, BP 48, 91192 Gif-sur-Yvette Cedex, France

David M. P. Holland
Daresbury Laboratory, Daresbury, Warrington, Cheshire WA4 4AD, United Kingdom

(Received 15 November 2016; revised manuscript received 15 June 2017; published 17 July 2017)

Vibrational state-resolved photoelectron anisotropy parameters, β, for the $\tilde{X}\,^2B_1$, $\tilde{B}\,^2B_2$, and $\tilde{C}\,^2B_1$ state ionizations of bromobenzene have been recorded at photon energies ranging from 20.5 to 94 eV, thus spanning the region of the expected bromine Cooper minimum (CM). The $\tilde{X}$ state displays no CM and its β value is also independent of vibrational level, in accord with the Franck-Condon approximation. The $\tilde{B}$ and $\tilde{C}$ state β values display the CM to differing degrees, but both show a vibrational dependence that extends to energies well below the obvious CM dip. Calculations are presented that replicate these observations. We thus demonstrate a wide-ranging Franck-Condon approximation breakdown detected in the β anisotropy parameter in the absence of any resonance. Measured and calculated vibrational branching ratios for these states are also presented. Although the $\tilde{B}$ state branching ratios remain constant, in accord with Franck-Condon expectations, the $\tilde{X}$ and (especially) the $\tilde{C}$ state ratios display weak, quasilinear variations across the studied range of photon energy, but with no apparent correlation with the CM position.

DOI: 10.1103/PhysRevA.96.013413

I. INTRODUCTION

The concept of the Cooper minimum is long established in the context of valence photoionization cross-section studies, but is receiving fresh attention in the investigation of high harmonic generation (HHG) [1]. In HHG the recollision of the laser-field-driven electron can be considered an inverse photoemission and so the Cooper minimum can be imprinted on the HHG spectral profile. As originally proposed [2] the Cooper minimum occurs in atomic ionization when the initial orbital possesses a radial node and the electric dipole matrix elements can be considered an r-weighted overlap integral that this orbital forms with the outgoing $\Delta l = \pm 1$ waves. As the electron energy increases, and the outgoing waves contract toward the core, the overlap integral in a given channel can change sign, the relevant matrix element consequently passing through a zero. At this point there will be a corresponding minimum in the total photoionization cross section.

The atomic photoelectron angular distribution can be even more strongly influenced by a Cooper minimum (CM) than is the cross section. Again this is readily understood in the atomic-like picture; for photoionization of a $3p$ electron there will be outgoing s and d waves, and as $3p \rightarrow kd$ amplitude gets canceled at the CM, the isotropic s wave alone remains to dominate, with the β anisotropy parameter consequently dipping to zero. In practice, however, the observed minima of cross section and β parameter may not exactly coincide [3].

The CM is also well established as a molecular phenomenon [4]. Most effort has been expended on identifying those instances of atomic-like behavior that can be associated with lone pair electrons localized on heavy atoms with, again, parallels in the context of current HHG developments [5]. While halogen-containing species have been at the heart of many such early investigations [4,6], other embedded heavy atoms such as S and Se have been examined [7]. Phenomenologically, the depth of a molecular CM, or even its absence, can be used to infer the degree to which atomic character of the initial orbital is suppressed by the mixing in of more delocalized molecular orbitals. This can be thought of as an initial state effect. At the same time the noncentral molecular potential scatters the outgoing electron into a greater range of outgoing channels with different phases, so that more complex interchannel interferences arise which are no longer just simple attenuation of a single channel. As a final state effect these interferences are reflected in the experimental observables such as depth and position of a CM, underscoring requirements for more fully developed theoretical understanding. For these more complex noncentral potential cases the angular distribution provides the favored CM diagnostic marker.

The outer valence orbitals of bromobenzene provide an interesting opportunity to examine molecular CM effects. The outermost benzene π-type orbitals are split, by the C_{2v} symmetry, into a $5b_1$ and $2a_2$ pair. The next-lying atomic Br $4p$ lone pair likewise splits into individual $8b_2$ and $4b_1$

*ivan.powis@nottingham.ac.uk
†Current address: Nano and Molecular Systems Research Unit, Molecular Materials Research Community, Faculty of Science, P.O. Box 3000, 90014 University of Oulu, Finland.
‡Current address: Institut für Chemie und Biochemie - Physikalische und Theoretische Chemie, Freie Universität Berlin, Takustr. 3, D-14195 Berlin, Germany.
§Current address: Extreme Light Infrastructure-Nuclear Physics (ELI-NP), "Horia Hulubei" National Institute for Physics and Nuclear Engineering, 30 Reactorului Street, RO-077125 Măgurele, Jud. Ilfov, Romania.

orbitals lying, respectively, in and out of the molecular plane and these can therefore interact in different degrees with the benzene ring electron density. One thus anticipates finding in these orbitals examples of either no, strong, or partial localization at the Br atom [8] and the β parameters associated with these outer four electronic bands in the photoelectron spectrum (PES) have been measured over extended photon energies (ranging up to 94 eV [9] or 120 eV [10]) to reveal modified molecular CM. Their interpretation clearly reflects these differences in localization and the one-particle, molecular orbital model for ionization holds well in these cases [8,10].

A different class of CM, with an intrinsically molecular origin, has also been identified in lighter molecules such as small hydrides [11,12], NO [13], and N_2 [14]. Since both initial and/or final state effects may be influenced by the molecular environment, a novel vibrational sensitivity was predicted in the vicinity of the CM in OH [12]. Subsequently, pioneering studies by Poliakoff and co-workers [15] have examined the dependence of the vibrational branching ratios through the N_2 $2\sigma_u^{-1}$ Cooper minimum. In the absence of resonant processes, such as autoionization and shape resonances, the Franck-Condon (FC) approximation predicts that vibrationally resolved branching ratios would be independent of electron (photon) energy. However, these experiments and modeling [15] showed a slow but definite variation of vibrational branching ratios, occurring over an extended excitation range of several tens of eV through the CM, and were interpreted as providing evidence for a wide-ranging, nonresonant FC violation.

The FC assumption of fully decoupled electron and nuclei motions also leads to a prediction that vibrationally resolved photoelectron anisotropy parameters, β, should display an energy dependence that was independent of the vibrational state. In this paper we seek, by measuring vibrationally resolved β anisotropy parameters and branching ratios, to further explore FC limitations while avoiding shape and autoionizing resonances. Recent high-resolution photoelectron studies of bromobenzene [9,16] have revised and extended the earlier vibrational analysis [10] of the outer valence bands. We now exploit the high resolution achievable at the PLÉIADES beamline (Synchrotron SOLEIL) to track the photoionization of these bands, maintaining full vibrational resolution across the extended photon energy range 20.5 to 94 eV. By recording angle-resolved PES we are able to extract vibrationally resolved β parameters completely spanning a molecular CM region.

II. METHODS

A. Experimental apparatus and procedure

The angle-resolved photoelectron spectra were recorded with a VG Scienta R4000 hemispherical electron energy analyzer mounted on the soft x-ray undulator based PLÉIADES beamline at the SOLEIL synchrotron radiation facility (France) [17]. Comprehensive descriptions of the monochromator, electron spectrometer, and experimental procedure have been given previously [9] so only those parameters affecting the overall resolution (which is the key factor in the present study) are discussed in detail here.

The beamline employs an HU256 electromagnetic undulator which provides linearly polarized radiation in the energy range 7–400 eV, with the degree of polarization being estimated as >99%. The plane of polarization can be chosen to lie either parallel or perpendicular to the plane of the electron orbit in the storage ring. Four varied line spacing, varied groove depth gratings are housed within a Petersen SX700 type monochromator [18]. The 400 lines/mm grating selected for our experiments, together with an exit slit width of 30 μm, results in a theoretical optical resolution which varies between 1 meV at $h\nu = 20$ eV and 4.5 meV at $h\nu = 82$ eV. However, the actual optical resolution varied from 5 to 11 meV. This was evaluated by fitting photoelectron spectra of the Kr^+ $(4p)^{-1}$ $^2P_{3/2}$ state to deconvolute the three contributions (monochromator resolution, electron spectrometer resolution, and Doppler broadening) determining the overall peak width.

The electron spectrometer was mounted in a fixed position, with photoionization occurring within a cell equipped with a series of electrodes to compensate for the so-called plasma potentials [19]. The analyser was used with a pass energy of 10 eV and a 0.2 mm curved entrance slit, resulting in a spectrometer resolution of 5 meV. The contribution ΔE_D, due to the translational Doppler broadening, to the overall resolution is given by $\Delta E_D = 0.7125\sqrt{\frac{E_{\mathrm{KE}}T}{M}}$ meV (where E_{KE} is the electron kinetic energy in eV, T is the absolute temperature of the sample gas, and M is the molecular mass expressed in atomic units [19]). For electrons ejected from bromobenzene with kinetic energies of 11 or 71 eV (corresponding to the formation of the $\tilde{X}$ $^2B_1$ state in the $v^+ = 0$ level using photon energies of 20 or 80 eV) the translational Doppler broadening ΔE_D is ~3.3 or ~8.4 meV, respectively.

Using the $\tilde{X}$ $^2B_1$ state photoelectron band as an example, the observed peak width associated with the principle vibrational progression varied between ~15 meV at low photon energies and ~40 meV at high photon energies. The separation between adjacent vibrational peaks was ~42 meV. Thus, across the excitation range relevant to the present experiment the overall resolution was sufficient to allow a detailed examination of the vibrational structure. This was crucial to the extraction of vibrationally resolved photoelectron anisotropy parameters and branching ratios.

Following several freeze-pump-thaw cycles of a commercial bromobenzene sample (Sigma-Aldrich, stated purity 99.5%), its vapor was admitted, at room temperature, into the ionization cell within the spectrometer.

At each photon energy, spectra were recorded for electrons emitted either parallel or perpendicular to the plane of polarization of the incident linearly polarized radiation. The orientation of this plane could be changed by varying the magnetic field in the undulator. Within the electric dipole approximation, and assuming randomly oriented target molecules, the photoelectron anisotropy parameter β associated with a particular vibrational state is given by

$$\beta = \frac{2(I_{\mathrm{par}} - I_{\mathrm{perp}})}{(I_{\mathrm{par}} + 2I_{\mathrm{perp}})}, \tag{1}$$

where I_{par} and I_{perp} are the photoelectron intensities corresponding to the appropriate vibrational peak, derived from

TABLE I. Regions of photoelectron spectrum selected for analysis.

Band	From (eV)	To (eV)	Peak no.	Assignment[a]
$\tilde{X}$				
	8.965	9.008	1	0–0
	9.008	9.050	2	11^1
	9.050	9.096	3	11^2
	9.096	9.141	4	11^3,...
	9.141	9.181	5	
	9.181	9.223	6	
$\tilde{B}$				
	10.578	10.663	1	0–0
	10.663	10.728	2	10^1
	10.728	10.768	3	9^1
	10.768	10.801	4	10^2,6^1
$\tilde{C}$				
	11.158	11.198	1	0-0
	11.198	11.230	2	11^1
	11.230	11.276	3	
	11.276	11.318	4	
	11.318	11.348	5	

[a]Where shown, this is the dominant transition assigned to the peak in Ref. [9].

spectra recorded in the parallel and perpendicular polarization geometries, respectively.

For a particular electronic state, the vibrational branching ratio is defined as the photoelectron intensity under the selected vibrational peak divided by the summation of the photoelectron intensity in all the vibrational peaks. The evaluation of the vibrational branching ratio requires knowledge of the transmission efficiency of the electron analyzer as a function of kinetic energy. This efficiency was determined by measuring the intensity ratio between photoelectron lines with varying kinetic energies and the corresponding constant kinetic energy Auger lines [20]. This procedure was carried out at various photon energies.

Vibrationally resolved photoelectron anisotropy parameters β and branching ratios for the $\tilde{X}\ ^2B_1$, $\tilde{B}\ ^2B_2$, and $\tilde{C}\ ^2B_1$ states were derived from the angle-resolved photoelectron spectra, after normalization to the sample pressure, the photon intensity and the acquisition time (all of which were monitored during data collection), and the analyzer transmission efficiency. Table I gives the binding energy ranges used to define the vibrational members within a specific photoelectron band. The vibrational branching ratios for a particular electronic state, given here, ignore peaks due to members not relevant to the present discussion. Hence, the vibrational branching ratios for the members of interest are normalized to unity.

The software employed to determine the intensity in a particular vibrational peak simply summed the electron counts within the binding energy range specified in Table I. No attempt was made to fit the vibrational profile. Such a procedure works well for the $\tilde{X}$ and $\tilde{B}$ bands where the first few vibrational peaks following that due to the adiabatic transition are dominated by contributions associated with one, or at most two, vibrational modes. It is less satisfactory for the $\tilde{C}$ band where the vibrational structure is more complicated [9,16].

B. Computational procedure

We incorporate vibrational influences into the calculation of β anisotropy parameters by evaluating the variation of the pure electronic dipole matrix elements with displacement of the nuclei along the vibrational coordinate. This approach has been previously used for the treatment of diatomic [12,21–25] and linear triatomic [26,27] molecular photoionization. An extension of this method to treat vibrational photoionization dynamics in polyatomic systems was recently described for a study of angular distribution parameters in chiral molecule photoionization [28], and here we adopt the same procedures to calculate $\beta(v)$ for bromobenzene.

In this approach the vibration specific matrix elements are obtained as

$$T_{i,f,v,v^+} = \int \mathcal{X}_{i,v}(Q) M_{i,f}(Q) \mathcal{X}_{f,v^+}(Q)\, dQ, \qquad (2)$$

with the electronic matrix element, written

$$M_{i,f}(Q) = \langle \psi_i(\mathbf{r}; Q) | \hat{\eta} | \psi_{f,\vec{k}}^{(-)}(\mathbf{r}; Q) \rangle_{\mathbf{r}}, \qquad (3)$$

having an explicit dependence on the vibration coordinate Q. Here $\hat{\eta}$ is the electric dipole operator, $\mathcal{X}_{i,v}$ and $\mathcal{X}_{f,v^+}$ are the corresponding vibrational wave functions, and ψ_i and $\psi_{f,\vec{k}}^{(-)}$ are the neutral and continuum (ionized) state electronic wave functions. Although retaining adiabatic separation of the full vibronic functions, it is the parametric dependence of the ψs on Q that couples electronic and nuclear motions; ignoring this dependence reverts to a FC approximation.

Harmonic normal mode vibrational analyses for the neutral and cation states were prepared using density functional theory (DFT) calculations with the B3LYP functional and cc-pVTZ basis, as implemented in the GAUSSIAN09 package [29]. For the excited state cations, time-dependent (TD-)DFT calculations were run using the same functional and basis. The displacement of a given cation's equilibrium geometry from that of the neutral ground state molecule can hence be expressed in the normal mode coordinates Q_m. A specific vibrational mode of interest n can then be selected for investigation, while all other modes are considered to be frozen. Using the calculated harmonic vibrational parameters and the displacement of the equilibrium geometry along Q_n it is hence possible to expand and evaluate the associated vibrational overlap function $\mathcal{X}_{i,v}(Q_n)\mathcal{X}_{f,v^+}(Q_n)$ appearing in Eq. (2).

The electronic matrix elements $M_{i,f}(Q_n)$ required for Eq. (2) are obtained by CMS-Xα calculations conducted at fixed points along Q_n with parameters chosen as previously described for fixed nuclei, equilibrium geometry calculations on bromobenzene [9]. The method for evaluating the weighted integration over Q_n [Eq. (2)] has likewise been previously described [24]. Once the full matrix elements T_{i,f,v,v^+} have been obtained, the corresponding β values are calculated using standard formulas [30] for randomly oriented molecular targets.

III. RESULTS

Figure 1 shows typical photoelectron data recorded at $h\nu = 40$ eV. Because of its relatively unstructured appearance the $\tilde{A}$ band will not be further discussed. The $\tilde{X}$, $\tilde{B}$, and $\tilde{C}$ PES bands have clear vibrational structures, which were assigned

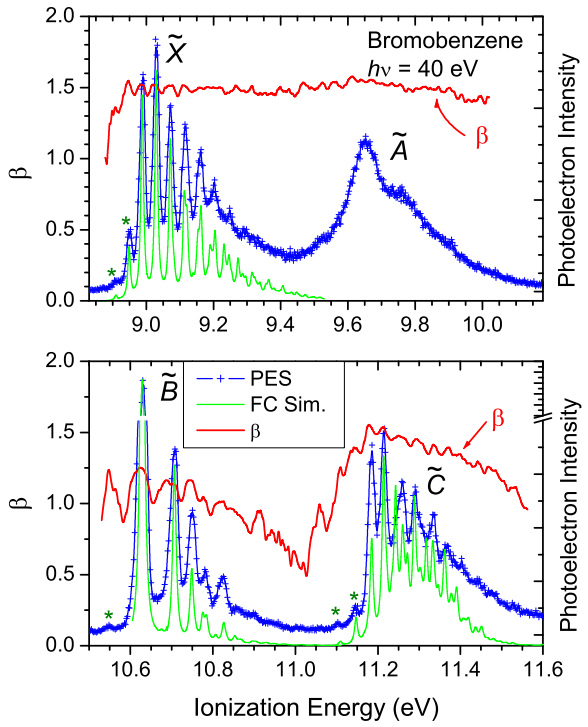

FIG. 1. Overview of the $h\nu = 40$ eV data. The "magic angle" photoelectron spectrum is reconstructed by combining scans recorded with parallel and perpendicular linearly polarized light, and the β parameter trace is similarly constructed from these recordings. Note the break in the vertical axis to truncate the intense origin of the $\tilde{B}$ band. A Franck-Condon simulation [9] is also shown with a small vertical offset for the vibrationally well-resolved $\tilde{X}$, $\tilde{B}$, and $\tilde{C}$ bands. Features assigned as vibrational hot bands are starred.

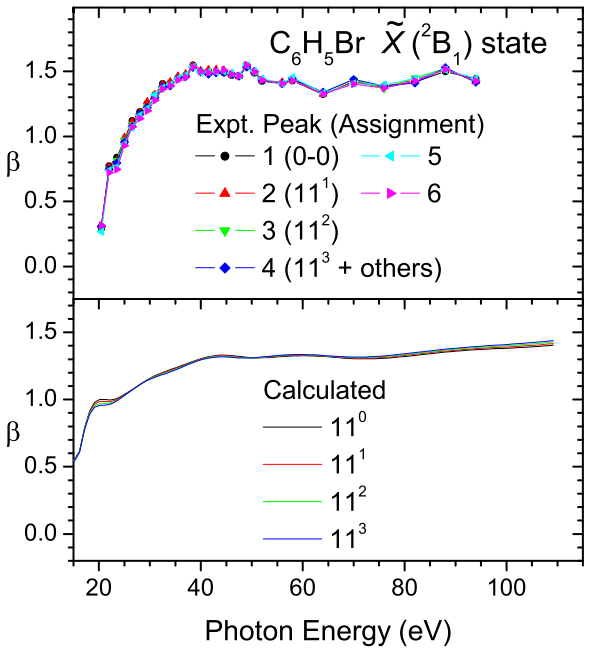

FIG. 2. Bromobenzene $\tilde{X}$ band $\beta(v)$. Top: experiment. Bottom: calculations for the C-Br stretch, ν_{11}.

[9,16] using FC simulations (included in Fig. 1). As will be seen, these bands also possess contrasting photoelectron angular distributions: $\tilde{X}$ ($5b_1$ ring π orbital) shows no indication of a CM, $\tilde{B}$ ($8b_2$ Br $4p\sigma$ in-plane lone pair orbital) displays a deep CM, while $\tilde{C}$ ($4b_1$ Br $4p\pi$ lone pair orbital) has an attenuated CM due to increased interaction of this out-of-plane Br $4p\pi$ orbital with the ring π orbitals [9,10].

A. $\tilde{X}$ band

Vibrationally resolved $\tilde{X}$ band β parameters measured across the photon energy range 20.5–94 eV are shown in Fig. 2, although hot band data have been omitted because of low intensity. The remaining peaks are predominantly a progression in the C-Br stretch, ν_{11}, although peaks 5 and 6 are composite multiple transitions [9,16]. Also shown in the figure are calculated β values for the $\tilde{X}$ state ν_{11} vibrational mode [31]. The clear conclusion from Fig. 2 is that β shows negligible experimental variation with vibrational peak, as also confirmed by the calculations.

Figure 3 shows experimental vibrational branching ratios obtained for the same $\tilde{X}$ band peaks. These are relatively featureless, although the peak 3 intensity increases slightly with photon energy relative to peaks 1 and 2. The calculated branching ratios (inset to Fig. 3) for the individual ν_{11} transitions are completely flat except for some weak structure at threshold. The vibrational invariance of the β parameters and an energy invariance of the branching ratios are as expected in the Franck-Condon approximation.

B. $\tilde{B}$ band

Figure 4, however, paints a different picture for the $\tilde{B}$ band Br $4p\sigma$ lone pair orbital. In addition to the intense Cooper minimum, the experimental β values now show a distinct vibrational dependence. To better examine this, by effectively expanding the vibrational differences across the photon

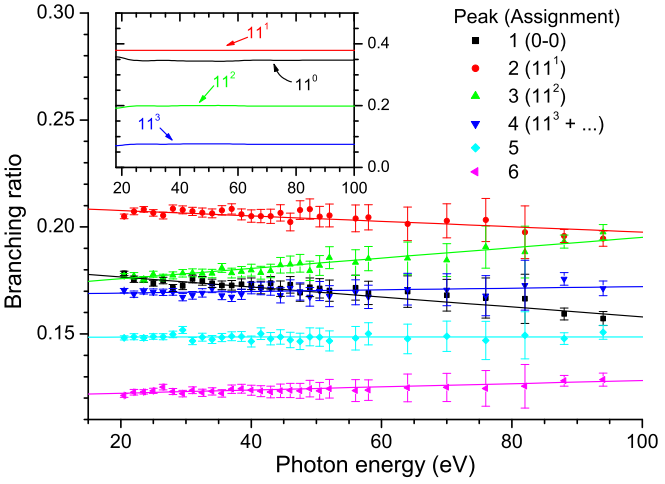

FIG. 3. Vibrational peak branching ratios for the bromobenzene $\tilde{X}$ band. Linear best fit lines are drawn through each of the data sets. The inset shows calculated branching ratios for the $\nu_{11} = 0$–3 transitions. Note that because of the different normalization over 4 transitions rather than 6 peaks the absolute magnitudes are not comparable with experiment.

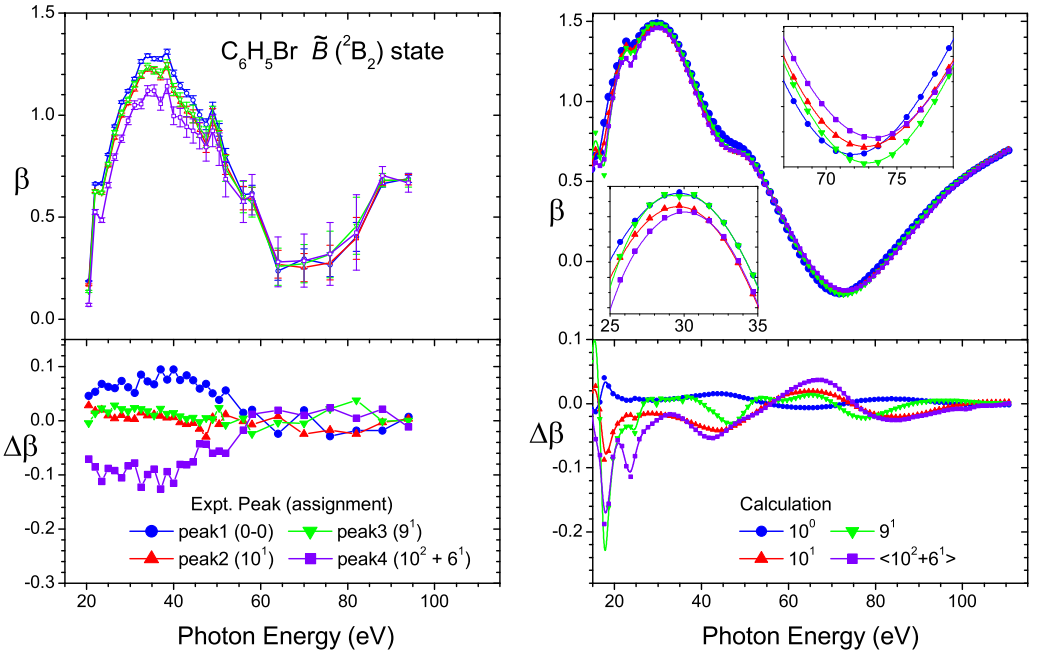

FIG. 4. $\tilde{B}$ state vibrationally resolved β parameters. On the left we show experiment, on the right calculation. Two insets (top right panel) show expanded views of the maxima and minima regions of the calculated curves. For the (unresolved) 10^2 and 6^1 excitations a simple average of the individual 10^2 and 6^1 calculated β is plotted. The lower panels show corresponding residuals, $\Delta\beta$ (see text).

energy range, Fig. 4 alternatively shows $\Delta\beta$, the vibrational residuals relative to a common reference curve (either the experimental mean β or the computed β obtained for a fixed equilibrium geometry calculation). Around $h\nu \approx 30$ eV, well below the obvious CM dip, a dispersion of the experimental β is clear, with $\beta(v = 0)$ spread to more positive values, the composite curve $\beta(v_{10} = 2, v_6 = 1)$ oppositely displaced in a negative direction, and $\beta(v_{10} = 1)$ and $\beta(v_9 = 1)$ being intermediate. In the visual CM dip at $h\nu \approx 70$ eV these experimental differences disappear, or possibly even reverse (unfortunately the error bars increase at higher energy because of decreasing cross section).

These trends, including the unanticipated vibrational dependence some tens of eV *below* the energy of the obvious CM dip, are well captured by the calculations. In particular the dispersion of the vibrational βs in the 20–50 eV range is semiquantitatively reproduced, albeit a little more structured than the experiment. The expanded insets in Fig. 4 show how the dispersion (ordering) of the vibrational βs switches between low and high photon energy regions, with a cross-over occurring at $h\nu \approx 55$ eV. From the inset showing the region around 72 eV it can be seen that both the position and depth of the CM are predicted to be vibration dependent. The predicted shifts of a few eV in the minima of successive ν_{10} vibrational levels considerably exceed the corresponding vibrational excitations. Hence these shifts are not simply attributable to consequent differences in electron energy, but must have a more fundamental origin. Furthermore, the differences evident in the $\nu_9 = 1$ curve clearly suggest there is also a *mode*-specific behavior in the CM dip. Unfortunately, this predicted detail cannot at present be confirmed from the experiments.

Branching ratios for the same four $\tilde{B}$ band peaks are presented in Fig. 5. Both theory and experiment show a negligible variation with photon energy. It may be noted that although the calculated ratios differ from experiment, this may be because the estimations of the latter inevitably include contributions from multiple unresolved weak transitions and hot bands underlying the main peaks.

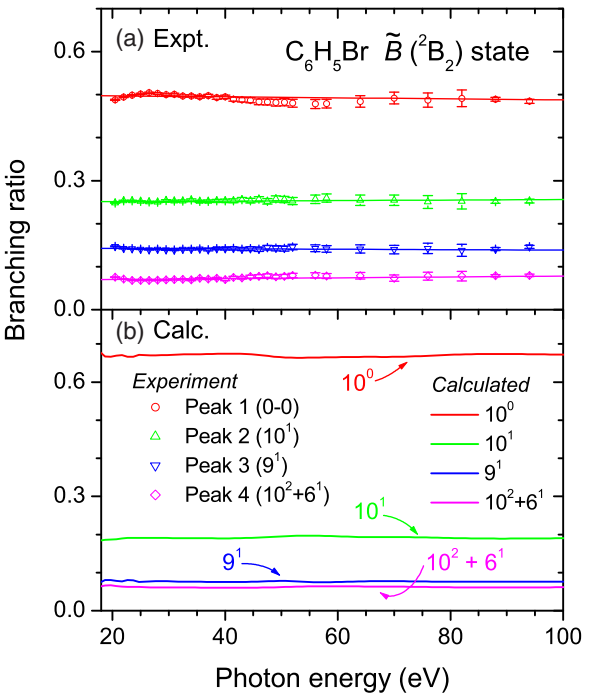

FIG. 5. $\tilde{B}$ state vibrational branching ratios. (a) Experimental values. The straight lines drawn through the vibrational data sets are linear best fits; (b) calculated ratios.

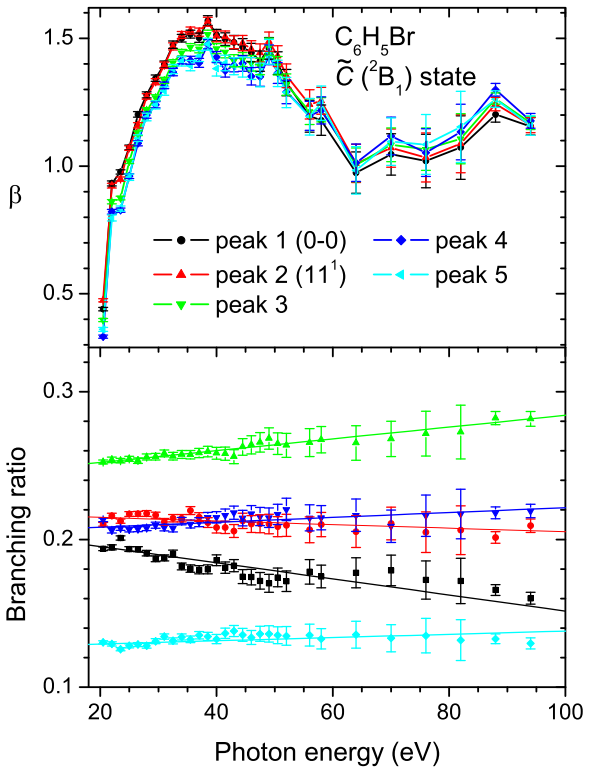

FIG. 6. $\tilde{C}$ state β parameters and vibrational peak branching ratios. For the latter, linear best fit straight lines are drawn through each vibrational data set.

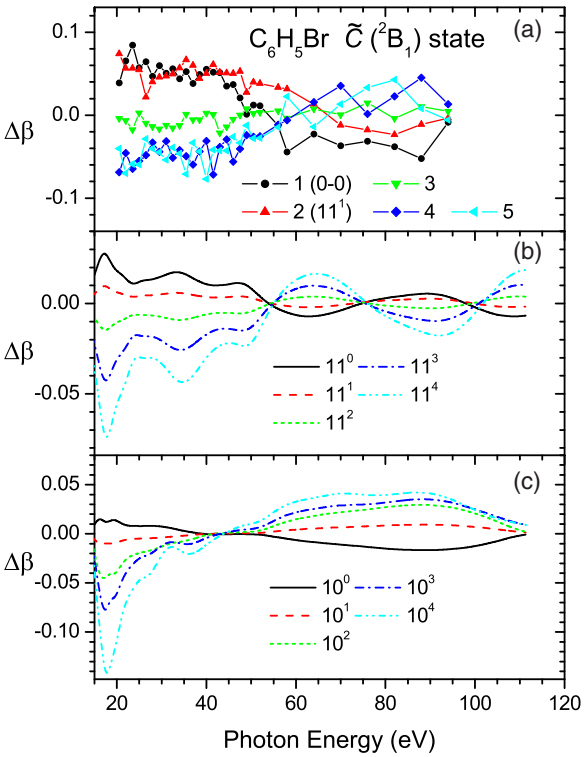

FIG. 7. (a) Experimental $\tilde{C}$ state residuals $\Delta\beta$ from the experimental mean β; (b), (c) residuals $\Delta\beta$ for calculated excitations of ν_{11} and ν_{10} levels (referenced from the β curve computed at a fixed equilibrium geometry).

C. $\tilde{C}$ band

The $\tilde{C}$ state ionization of an out-of-plane Br $4p\pi$ lone pair electron displays a weaker β CM. From the vibrationally unresolved electronic band measurements, it was deduced that this attenuation reflects an increased electron delocalization due to interaction with ring π electrons [9]. This delocalization was evidenced in a Mulliken population analysis [8] and is similarly indicated by a reduction in the normalized electron density on the Br atom obtained in the MS-Xα calculations conducted here (0.35 for the $4b_1$ π_{BrLP} orbital compared to 0.77 for the $8b_2$ σ_{BrLP} orbital).

Compared to the $\tilde{X}$ and $\tilde{B}$ states, the $\tilde{C}$ state PES band vibrational intensities were less well reproduced by FC simulations [9,16]. The main predicted progressions comprise excitation of the ν_{11} C-Br stretch, either singly or in combination with the ν_{10} mode, but relative intensities of the ν_{11} transitions are overestimated while predicted spacings are also weakly perturbed. Consequently, it is difficult to reliably assign beyond the first adiabatic (0-0) and second (11^1) peaks. The underlying reasons are unclear. Palmer *et al.* [16] have nevertheless inferred an absence of vibronic interaction with nearby states, given similar vibrational linewidths in the other PES bands. However, from the better resolution in our own study [9] it is clear that their linewidths were instrumentally limited, so this inference may not be valid.

Experimental branching ratios and anisotropy parameters, β, for the first five $\tilde{C}$ band vibrational peaks are shown in Fig. 6. While not as completely flat (constant) as the $\tilde{B}$ state ratios (Fig. 5) the variation of the vibrational branching is quite linear across the full photon energy range, and there is again nothing to suggest a CM-influenced branching behavior. However, the vibrational peak resolved β parameters again show a strong dispersion at energies both *below* and through the CM region, paralleling the $\tilde{B}$ band results in (Fig. 4).

These variations are more closely examined in Fig. 7 by plotting the experimental residuals, $\Delta\beta$, and corresponding calculations that treat the two most prominent vibrational modes, ν_{10}, ν_{11}, excited in this cationic state [9]. There is a striking similarity in the β dispersion in the range 20–55 eV, both in experiment and in the calculations for the dominant ν_{11} vibrational mode. At ~55 eV both also pass through some form of cross-over above which, in the CM region, the ν_{11} calculations shows structured, oscillating β dispersions. In contrast the ν_{10} calculations show simpler behavior, with β being displaced to more positive values for progressively higher vibrational excitations but with no further switching of this relative order across the 55–100 eV region. This looks rather more like the experimental behavior in the same region. Below 45 eV the ν_{10} β curves are spread in a reversed sense, similar now to both the ν_{11} and the experimental results.

IV. CONCLUSIONS

At the heart of our study has been the measurement of vibrationally resolved angular distribution β parameters and relative cross sections (branching ratios) across a very wide photon energy range. We have examined bands in the photoelectron spectrum of bromobenzene that display either

a strong, weak, or no Cooper minimum. There is no obvious vibrational dependence of β for the $\tilde{X}$ band, which lacks a CM, suggesting uncoupled electron and nuclear motion as implied by the full FC approximation.

For the $\tilde{B}$ state, which has an intense, deep CM in the photoelectron angular distribution, the calculations indicate vibrational state sensitive position and depth of the CM (Fig. 4 insets), indicative of the FC breakdown we initially anticipated. The experimental observations confirm that β has a vibrational sensitivity in the CM region, although unfortunately the statistical quality is insufficient to verify the specific detail that is predicted. On the other hand, both the simulated and experimental vibrational branching ratios are completely flat across the CM region (Fig. 5), betraying no influence of changing dynamics. Following established understanding [3,32,33] such contrasting sensitivities of cross section and angular distribution can be attributed to the former's nondependence upon phase; implying that the β parameter vibrational changes are due to varying phases of the photoelectron partial waves.

A somewhat similar commentary may be applied to describe the $\tilde{C}$ state CM region results. Here, some of the experimental branching ratios do now show a weak linear variation with photon energy, but there is again no structure that correlates with the visually apparent CM dip in the $\tilde{C}$ state βs. However, an unanticipated finding for both $\tilde{B}$ and $\tilde{C}$ states is that the vibrational dependence of the β parameters is even more marked in the 20–50 eV photon energy range, so commencing at energies that are well below the apparent CM energy dip. These experimental observations are equally well reproduced in the calculations that have been performed.

We thus are able to demonstrate for the first time FC breakdown affecting photoelectron angular distributions occurring across an extended photon energy without there being a resonance. On the other hand our observations on the vibrational branching ratios do not so directly challenge FC assumptions, at least not for the $\tilde{B}$ state.

An expected prerequisite for the occurrence of the CM in these valence bands is a strong localization of the initial orbital on the peripheral Br atom. This localization may generally enhance the vibrational sensitivity induced by nuclear motion (specifically that of near-neighbor photoelectron scattering sites in the molecular ion potential), and in this sense might prove more pertinent than just the consequent CM phenomenon, exerting influence across an even wider energy range. Nevertheless, both the $\tilde{B}$ band (Fig. 4 insets) and, especially, the $\tilde{C}$ band (Fig. 7) results hint at unexpected patterns of vibrational *mode*-specific variation in the region of the actual CM dip that are not yet understood and merit further investigation.

ACKNOWLEDGMENTS

This research was funded by the European Community's Seventh Framework Program (FP7/2007-2013) ELISA under Grant Agreement No. 226716. We are grateful to SOLEIL staff for running the facility and providing beam time (Project No. 20120162).

[1] A. D. Shiner, B. E. Schmidt, C. Trallero-Herrero, P. B. Corkum, J. C. Kieffer, F. Legare, and D. M. Villeneuve, J. Phys. B: At. Mol. Opt. Phys. **45**, 074010 (2012); M. Ruberti, V. Averbukh, and P. Decleva, J. Chem. Phys. **141**, 164126 (2014); S. B. Schoun, R. Chirla, J. Wheeler, C. Roedig, P. Agostini, L. F. DiMauro, K. J. Schafer, and M. B. Gaarde, Phys. Rev. Lett. **112**, 153001 (2014); F. Cloux, B. Fabre, and B. Pons, Phys. Rev. A **91**, 023415 (2015).

[2] J. W. Cooper, Phys. Rev. **128**, 681 (1962).

[3] U. Becker and D. Shirley, in *VUV and Soft X-Ray Photoionization*, edited by U. Becker and D. A. Shirley (Plenum, New York, 1996), Chap. 5, pp. 135–180.

[4] T. A. Carlson, M. O. Krause, W. A. Svensson, P. Gerard, F. A. Grimm, T. A. Whitley, and B. P. Pullen, Z. Phys. D: At. Mol. Clusters **2**, 309 (1986).

[5] M. C. H. Wong, A. T. Le, A. F. Alharbi, A. E. Boguslavskiy, R. R. Lucchese, J. P. Brichta, C. D. Lin, and V. R. Bhardwaj, Phys. Rev. Lett. **110**, 033006 (2013).

[6] T. A. Carlson, A. Fahlman, M. O. Krause, T. A. Whitley, and F. A. Grimm, J. Chem. Phys. **81**, 5389 (1984).

[7] I. Powis, J. D. Thrower, A. B. Trofimov, T. E. Moskovskaya, J. Schirmer, A. W. Potts, D. M. P. Holland, F. Bruhn, and L. Karlsson, Chem. Phys. **315**, 121 (2005); I. Powis, I. L. Zaytseva, A. B. Trofimov, J. Schirmer, D. M. P. Holland, A. W. Potts, and L. Karlsson, J. Phys. B: At. Mol. Opt. Phys. **40**, 2019 (2007).

[8] M. Schneider, D. Y. Soshnikov, D. M. P. Holland, I. Powis, E. Antonsson, M. Patanen, C. Nicolas, C. Miron, M. Wormit, A. Dreuw, and A. B. Trofimov, J. Chem. Phys. **143**, 144103 (2015).

[9] I. Powis, D. M. P. Holland, E. Antonsson, M. Patanen, C. Nicolas, C. Miron, M. Schneider, D. Y. Soshnikov, A. Dreuw, and A. B. Trofimov, J. Chem. Phys. **143**, 144304 (2015).

[10] D. M. P. Holland, D. Edvardsson, L. Karlsson, R. Maripuu, K. Siegbahn, A. W. Potts, and W. von Niessen, Chem. Phys. **252**, 257 (2000).

[11] K. H. Wang, J. A. Stephens, and V. McKoy, J. Phys. Chem. **98**, 460 (1994).

[12] J. A. Stephens and V. McKoy, Phys. Rev. Lett. **62**, 889 (1989).

[13] K. Wang, J. A. Stephens, and V. McKoy, J. Chem. Phys. **95**, 6456 (1991).

[14] J. B. Bertrand, H. J. Worner, P. Hockett, D. M. Villeneuve, and P. B. Corkum, Phys. Rev. Lett. **109**, 143001 (2012).

[15] R. M. Rao, E. D. Poliakoff, K. H. Wang, and V. McKoy, Phys. Rev. Lett. **76**, 2666 (1996); J. Chem. Phys. **104**, 9654 (1996); J. A. Lopez-Dominguez, D. Hardy, A. Das, E. D. Poliakoff, A. Aguilar, and R. R. Lucchese, J. Electron Spectrosc. Relat. Phenom. **185**, 211 (2012).

[16] M. H. Palmer, T. Ridley, S. V. Hoffmann, N. C. Jones, M. Coreno, M. de Simone, C. Grazioli, T. Zhang, M. Biczysko, A. Baiardi, and K. Peterson, J. Chem. Phys. **143**, 164303 (2015).

[17] J. Söderström, A. Lindblad, A. N. Grum-Grzhimailo, O. Travnikova, C. Nicolas, S. Svensson, and C. Miron, New J. Phys. **13**, 073014 (2011).

[18] H. Petersen, Opt. Comm. **40**, 402 (1982).
[19] P. Baltzer, L. Karlsson, M. Lundqvist, and B. Wannberg, Rev. Sci. Instrum. **64**, 2179 (1993).
[20] J. Jauhiainen, A. Ausmees, A. Kivimäkia, S. J. Osborne, A. N. de Brito, S. Aksela, S. Svensson, and H. Aksela, J. Electron Spectrosc. Relat. Phenom. **69**, 181 (1994).
[21] D. A. Mistrov, A. De Fanis, M. Kitajima, M. Hoshino, H. Shindo, T. Tanaka, Y. Tamenori, H. Tanaka, A. A. Pavlychev, and K. Ueda, Phys. Rev. A **68**, 022508 (2003).
[22] S. K. Semenov, N. A. Cherepkov, T. Jahnke, and R. Dorner, J. Phys. B: At. Mol. Opt. Phys. **37**, 1331 (2004).
[23] M. Hoshino, R. Montuoro, R. R. Lucchese, A. De Fanis, U. Hergenhahn, G. Prumper, T. Tanaka, H. Tanaka, and K. Ueda, J. Phys. B: At. Mol. Opt. Phys. **41**, 085105 (2008).
[24] I. Powis, Phys. Rev. A **84**, 013402 (2011).
[25] E. Plesiat, P. Decleva, and F. Martin, Phys. Chem. Chem. Phys. **14**, 10853 (2012).
[26] R. R. Lucchese, J. Soderstrom, T. Tanaka, M. Hoshino, M. Kitajima, H. Tanaka, A. De Fanis, J. E. Rubensson, and K. Ueda, Phys. Rev. A **76**, 012506 (2007).
[27] A. Das, E. D. Poliakoff, R. R. Lucchese, and J. D. Bozek, J. Chem. Phys. **130**, 044302 (2009).
[28] G. A. Garcia, H. Dossmann, L. Nahon, S. Daly, and I. Powis, Chem. Phys. Chem. **18**, 500 (2017).
[29] M. J. Frisch, G. W. Trucks, H. B. Schlegel, G. E. Scuseria, M. A. Robb, J. R. Cheeseman, G. Scalmani, V. Barone, B. Mennucci, G. A. Petersson, H. Nakatsuji, M. Caricato, X. Li, H. P. Hratchian, A. F. Izmaylov, J. Bloino, G. Zheng, J. L. Sonnenberg, M. Hada, M. Ehara, K. Toyota, R. Fukuda, J. Hasegawa, M. Ishida, T. Nakajima, Y. Honda, O. Kitao, H. Nakai, T. Vreven, J. J. A. Montgomery, J. E. Peralta, F. Ogliaro, M. Bearpark, J. J. Heyd, E. Brothers, K. N. Kudin, V. N. Staroverov, T. Keith, R. Kobayashi, J. Normand, K. Raghavachari, A. Rendell, J. C. Burant, S. S. Iyengar, J. Tomasi, M. Cossi, N. Rega, J. M. Millam, M. Klene, J. E. Knox, J. B. Cross, V. Bakken, C. Adamo, J. Jaramillo, R. Gomperts, R. E. Stratmann, O. Yazyev, A. J. Austin, R. Cammi, C. Pomelli, J. W. Ochterski, R. L. Martin, K. Morokuma, V. G. Zakrzewski, G. A. Voth, P. Salvador, J. J. Dannenberg, S. Dapprich, A. D. Daniels, O. Farkas, J. B. Foresman, J. V. Ortiz, J. Cioslowski, and D. J. Fox,*Gaussian 09 revision d.01* (Gaussian Inc., Wallingford, CT, 2013).
[30] D. Dill and J. L. Dehmer, J. Chem. Phys. **61**, 692 (1974).
[31] The notation m^n as used here indicates vibrational mode m and level n excited in the ion. For experiment the adiabatic (vibrationless) excitations are alternatively labeled 0-0, but for the calculated quantities we retain the notation m^0 since while zero point motion of the mode m is included, all other modes are considered frozen. Hence calculations for the nominally vibrationless excitation of the ion may nevertheless have some dependence on the selected mode m.
[32] J. Cooper and R. N. Zare, J. Chem. Phys. **48**, 942 (1968).
[33] D. Dill, Phys. Rev. A **7**, 1976 (1973).